August 2016

Rational Design of Cathode Materials for High Performance Lithium-Sulfur Batteries

Xi Chen
University of Wisconsin-Milwaukee

RATIONAL DESIGN OF CATHODE MATERIALS FOR HIGH PERFORMANCE LITHIUM-SULFUR BATTERIES

by

Xi Chen

A Thesis Submitted in

Partial Fulfillment of the

Requirements for the Degree of

Master of Science in

Engineering

at

The University of Wisconsin-Milwaukee

August 2016

ABSTRACT

RATIONAL DESIGN OF CATHODE MATERIALS FOR HIGH PERFORMANCE LITHIUM-SULFUR BATTERIES

by

Xi Chen

The University of Wisconsin-Milwaukee, 2016

Under the Supervision of Professor Junjie Niu

Sulfur, one of most promising cathode candidates for next-generation lithium ion batteries, shows a limited cycling performance due to its shuttling effect, low conductivity, self-discharge and volume expansion during lithiation and delithiation process. According to the operation principles, failure mechanism, and recent progress on lithium-sulfur batteries, here we developed several scalable and rational synthesis methods for high performance cathode materials. We dissolved commercial sulfur to anhydrous ethylenediamine (EDA) to form an EDA-S precursor, and then we reduced the sulfur particles size at conductive carbon black substrate. The 70% theoretical capacity of sulfur cathode battery was obtained. We also melted commercial sulfur into conductive carbon black matrix, the nanosponge carbon sulfur composite was successfully synthesized. Characterization techniques (XRD, SEM, TEM) were used to check the structure and morphology of the received materials. Coin cell battery cyclic voltammetry (CV) and cycling performance were used for electrochemical measurements.

TABLE OF CONTENTS

LIST OF FIGURES

LIST OF TABLES

LIST OF ABBREVIATIONS

CV	Cyclic voltammetry
EDS	Energy-dispersive X-ray spectroscopy
EDA	Ethylenediamine
Li-ion	Lithium-ion
LIBs	Lithium-ion batteries
Li-S	Lithium sulfur
$LiNO_3$	Lithium nitrate
$LiMO_2$	Lithium transition-metal oxide
LFP	Lithium iron phosphate
NMP	N-methyl-2-pyrrolidone
NWs	Nanowires
ORR	Oxygen reduction reaction
PE	Polyethylene
PP	Polypropylene
SEM	Scanning electron microscopy
TEM	Transmission electron microscopy
XRD	X-ray diffraction

ACKKNOWLEDGEMENTS

I want to say thank to my advisor, Professor Junjie Niu, for his support and advice to complete my master thesis. Under his guidance, I became interested in research. Also I learned from him that the most important thing for research and academic is rigorous.

Then, I would like to thank Prof. Church and Prof. Wang. I appreciate your advising in my thesis defense and dissertation.

Also, I sincerely thank all postdocs and students in Dr.Niu's group. All the specific help in experiments from you are indispensable. You always encourage me when I face challenge in experiments.

I want to thank everyone who helped me during my master study in UW-Milwaukee.

Last, thousands of words would not be enough to thank my family, I love you.

1. Introduction

Energy storage system plays an important role in engineering field, since energy shortage and environmental pollution are major issues in 21st century. Various advanced energy storage system such as batteries, fuel cells and capacitors coexist in engineering research area to solve the problems we've faced. Higher specific energy density, specific power density, volumetric energy density and volumetric power density imperatively need to be improved for further applications in industries and daily life. Battery as one of most promising candidate in energy storage system has enormous potential to improve. The existing mainly conventional rechargeable batteries, including, nickel cadmium batteries, nickel metal hydride batteries and lead- acid batteries are well developed. Research popularity in lithium-ion (Li-ion) batteries (LIBs) continuously improved recent decades due to its high specific energy density, high open-circuit voltage, and high output power, wide working temperature range, low discharge rate, no memory effect, long cycle performance and environment friendly compared with other batteries. Since the LIBs have been proposed in 1976 by M.S.Whittingham[1] and decades improvement by other engineers and researchers, its integral performance had a tremendous improvement. LIBs have been commercialized for more than 20 years. Now it has a widely applications in mobile phones, laptops and portable electronics. Also the future demand for electronic vehicles and large scale energy storage system prompted the rapid development of lithium batteries. Highly performance LIBs and novel electrode materials presented recent years. LIBs research can be called prosperity, the system including Li-S, Li-Metal, and Li-Si and Li-Air system light up the diversified development direction of lithium batteries.

1.1 Lithium-Ion Batteries

In Li-ion batteries, lithium ions move from the anode to cathode during discharge, and move from cathode to anode when charging. The anode materials, cathode materials and electrolyte play a critical role to affect the performance of lithium ion batteries, including capacity, cycle life and operation environment etc. New electrode materials with high capacities and long cyclic performance attract a lot of attention from researchers. Nowadays, energy density of batteries cannot meet the demand of the mobile electricity device, which prompts an urgent improvement in lithium ion batteries.

1.1.1 Principles of Lithium-Ion Batteries

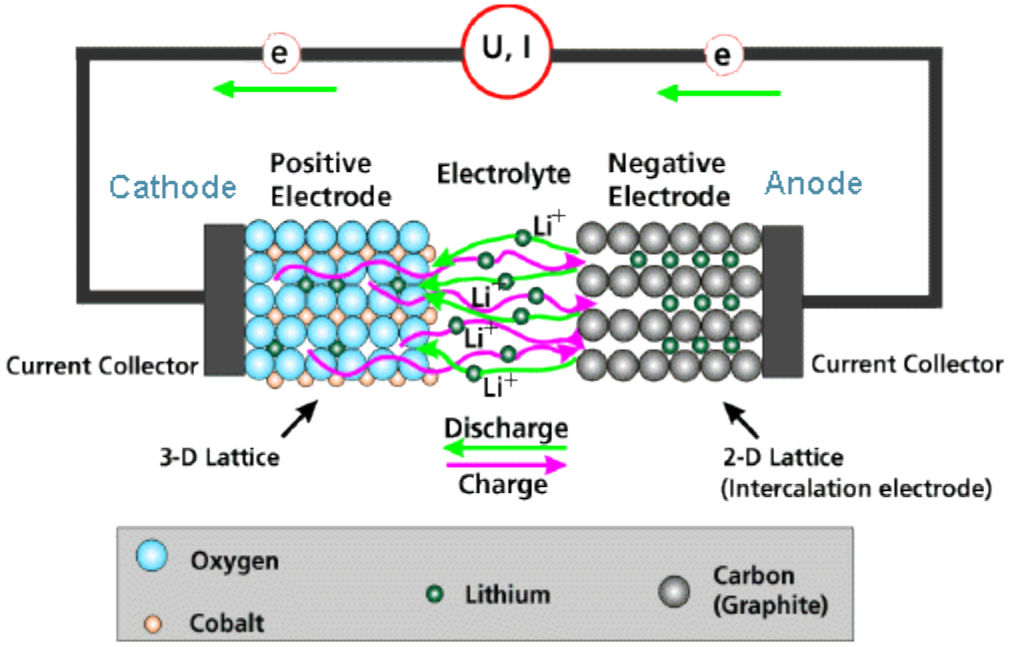

Figure 1.1 Operating mechanism of conventional graphite-$LiCoO_2$ system (courtesy from aventurine.com)

Figure 1.1 is a graphic illustration of lithium-ion battery (LIB). A conventional LIB constitute from graphite anode, lithium metal oxide (the most common type are $LiCoO_2$, $LiMn_2O_4$ and $LiFePO_4$) cathode, electric insulating and lithium ion conducting separator and organic electrolyte. The charge-discharge process also is called delithition-lithiation process, the lithium ions can pass through the separator and electrolyte with lithium salt. Lithium ions can electrochemically react with electrodes materials and generate the electrons. For example of $LiCoO_2$ as cathode, the electrochemical reaction process between graphite anode and lithium cobalt oxide cathode can be expressed as following equations:

The positive electrode reaction:

$$LiCoO_2 \leftrightarrow Li_{1-x}CoO_2 + xLi + xe^- \qquad (1)$$

The negative electrode reaction:

$$xLi + xe^- + xC_6 \leftrightarrow xLiC_6 \qquad (2)$$

The overall reaction:

$$LiCoO_2 + xC_6 \leftrightarrow xLiC_6 + Li_{1-x}CoO_2 \qquad (3)$$

The electrode materials are one of most impact factor for energy storage, the specific capacities of an electrode materials highly depend on composition and morphology of electrode materials. Both electrodes are produced from active materials mixed polymer binder (mostly polyvinylidene fluoride, PVDF) and conductive carbon additives (mostly conductive carbon black) and coated on one side or both sides of current collector foils (aluminum foil for cathode and copper foil for anode).

1.1.2 Advanced Anode Materials

Silicon Anode Materials

Silicon is a hot research direction for anode materials, Since it has ultra-high theoretical

capacity (3,579 mAh g^{-1}, in pure phase of $Li_{22}Si_5$) and volumetric capacity (9,786 mAh cm^{-3}) [2]compare with the other anode material candidates.

Besides, the lithiation potential of silicon is slightly higher than graphite (0.07), silicon is 0.22 V when Li^+/Li as reference.[2] Therefore, silicon anode has less chance for dendrite growth during the lithiation and delithiation process. So the better safety performance is another advantage for silicon anode.

The mechanism of Si anode electrochemical reaction had been detailed investigated by researchers and scholars for decades. The high specific capacity for silicon anode is provided by formation of intermetallic Li–Si binary alloys such as $Li_{12}Si_7$, Li_7Si_3 and $Li_{13}Si_4$ first and later $Li_{22}Si_5$ metastable crystalline formed.[3] But, drastically volume change induced poor cycling performance is major disadvantage of silicon-based anode materials. According to literature, volume expansion during alloying and dealloying of lithium silicon batteries is about 400%, which easily result in pulverization for structure of silicon materials.

To accommodate the volume expansion during the alloying/de-alloying process, the nanowires, nanotubes and yolk shell silicone particles were designed by researchers. In literature, Si nanowires (Si NWs) and nanotube perform a reversible high capacity over 2000 mAh/g. The capacity of yolk shell silicon particles have reached to 2500 mAh/g with good cycling stability.[4] Nano sized silicon particles have ultra-high capacity close to theoretical capacity. The critical size for ultra-high capacity silicon anode is 10nm with carbon coating.[5] The flexible conductive shell can accommodate volume expansion also play a critical role to enhance the performance of silicon anode.[6] The electrode materials with nanosized particles and conductive additive always are able to effectively improve the overall performance.

Tin Anode Materials

Tin has a high specific capacity of 990 mAh g^{-1} in fully lithiated Li22Sn5 alloy. Therefore, tin anode also is a promising anode candidate which attracted attention from researchers. Like silicon, reversible alloying and dealloying phase with different composition including Li_2Sn_5, LiSn, Li_7Sn_3, Li_5Sn_2, Li_7Sn_2, $Li_{13}Sn_5$ and $Li_{22}Sn_5$. But research of tin anode doesn't fully like silicon; it has much focus on tin oxides which can drastically increasing the cyclic performance.[7] The pure tin anode doesn't have a stable cyclic performance because of high frangibility. The volume expansion induced mechanical failure can be observed in 10 nm size Sn particles.[8] So the tin anode with tin oxides phase doped inside was suggested to be ideal electrode materials. The tin oxide can hold all the tin phase together during lithiation and delithiation.[9]

Tin has low melting point with 232 °C, so tin atoms has better mobility at room temperature compared with materials has high melting point. So crystallization is much easier for tin at room temperature. During the lithiation process, lithium ions embed into tin, and tin atoms will easily shift the original position due to not enough space for lithium-tin alloys. This could be a good explanation for fracturing of tin anode. Binder doped tin oxide composites materials is an ideal solution for tin anode.

Tin oxide received highly attention since commercial development by Fujifilm corporation and science paper from Idota el.[10] And high theoretical capacity and low operation voltage of 0.6 V vs. Li/Li^+ are advantages for tin oxide.[11] The in-situ XRD electrochemical test already revealed lithium alloying and dealloying reactions for tin oxide in 1997. It can be detected by XRD first irreversible step and second reversible step. The irreversible lithiation process is SnO_2 is reduced to tin and lithium oxides ($SnO_2 + 4Li \leftrightarrow Sn + 2Li_2O$), the following reversible lithiation process is tin and lithium alloying/de-alloying reaction ($Sn + 4.4Li \leftrightarrow Li_{4.4}Sn$).[12] Also, there are some researchers give a higher delithiation potential to surpass the theoretical capacity of tin

anode by reversing lithiation process of Li_2O. An tin oxide anode with reversible Li_2O by using high surface area graphene can deliver a high capacity of 1100 to 1400, good cyclic performance and rate performance.[13]

However, tin or tin oxides materials have the same challenge, it is volume expansion induced structure fragmentation, resulting in low cyclic performance.[14] The major research trend is to find the ways to minimize the effect of volume change and extend the cyclic durability. Yolk-shell nanoparticles, porous nanostructures, graphene based nanocomposites Sn/SnO_2 have been done to accommodate the volume expansion caused failure.[15]

1.1.3 Advanced Cathode Materials

Cathode materials also play an important role in LIBs. Lithium oxides compounds were well developed by scientist in 1980. Crystallization of lithium oxides compounds could provide fair lithium ions mobility during the redox reaction. Cathode materials especially oxides compounds have a stable crystal structure and minimum volume expansion during lithiation and delithiation process. They have good adaptability at an entire voltage range of lithium insertion and extraction. So it can provide a good cyclic performance. Nowadays, more and more novel cathode materials based on high energy density attracted attention from researchers, such as lithium-sulfur batteries system and lithium air batteries system.

Lithium Cobalt Oxide ($LiCoO_2$)

$LixCoO_2$ becomes the well-known cathode electrode materials with good conductivity and Li ion mobility in LIBs for decades. Todays, it is still a widely commercial used cathode material for LIBs. In theoretical, lithium cobalt oxide has a high specific capacity with 274 mAh/g with respect to full delithiation of Li ion extraction and producing CoO_2.[16] But in reality, full lithiation

is not reversible process in Li_xCoO_2. In practical, x=0.5 induced capacity loss with value of 140mAh/g.[17] Also layered compounds structural is a significant characteristic for LiCoO2. It is most widely accept cathode materials in LIBs.

Lithium Iron Phosphate (LFP)

LFP is another commercialized cathode materials with olivine structure in lithium ion batteries. It still attracted attention from researchers due to the inexpensive and naturally abundant. But low ionic and electrical conductivity are major disadvantages for LFP. So to improve high rate capability and long cyclic performance by carbon coating, size reduction and morphology modification still are research interests for researchers.[18] Besides, mechanism of phase transformation during lithiation and delithiation process is another research interests.[19]

Lithium-Air Batteries

One of the novel cathode materials research recent years in LIBs is lithium-air batteries. The cathode lithium oxygen reaction can provide a high theoretical capacity of 3.5kWh/kg nonaqueous lithium oxygen battery.[20] The major cathode product material is lithium peroxide. The cathode oxygen reduction reaction (ORR) is $O_2 + 2Li^+ + 2e^- \rightarrow 2Li_2O_2$, which has overall equilibrium potential of 2.96V versus lithium metal. However, the poor cyclic performance, slowly charging/discharging rate, high overpotential and low energy efficiency are major problems for lithium-air batteries. Generally, the lithium air batteries performance highly depends on the products created in cathode during lithiation and delithiation process. The morphology of cathode reaction products, the morphology of peroxide effect on batteries performance and fabricated high performance cathode are hot research topics on lithium air batteries.[21] According to literature and Figure 1.2, there are many approaches to design an ideal cathode for lithium air batteries.[22] For instance, the porous structures with appropriate pore size,

to improve reaction kinetics by catalyst and oxygen diffusion and to improve electrical conductivity are major strategies.

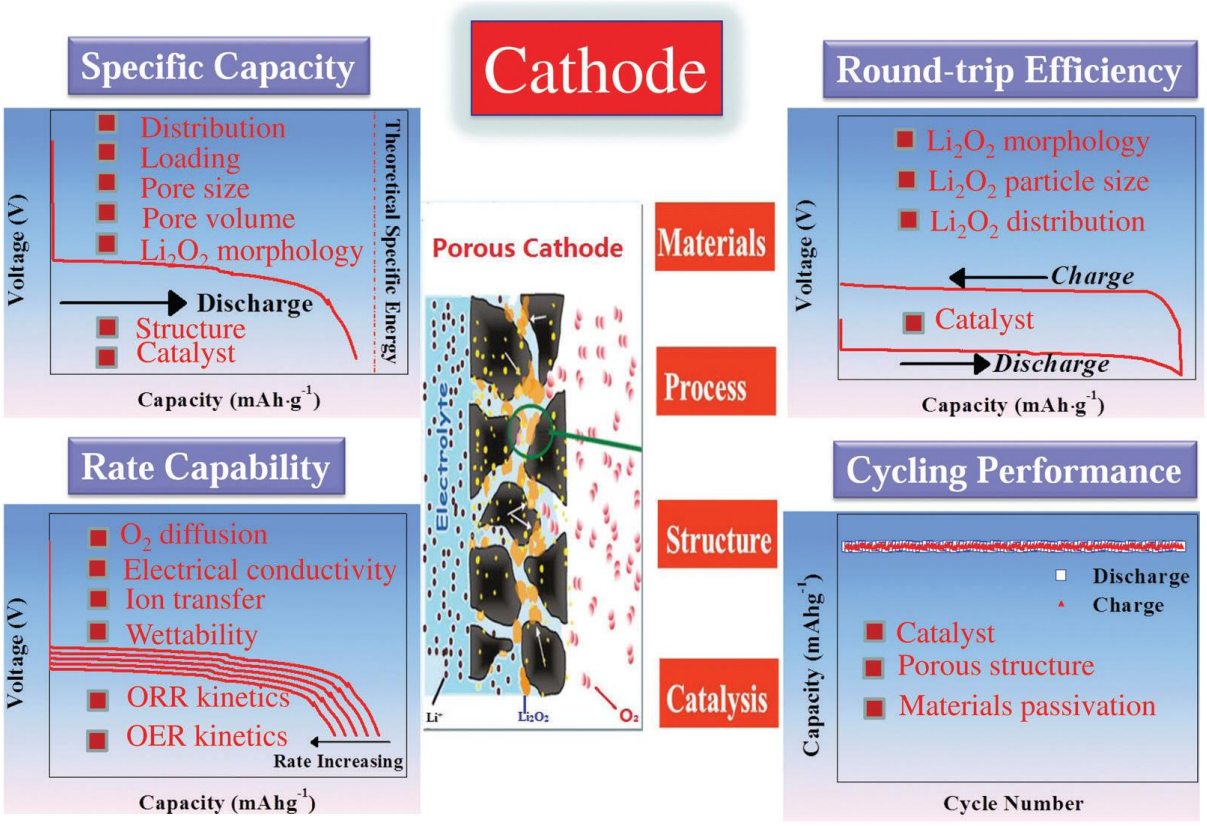

Figure 1.2 Ideal cathode designing strategies for lithium-air batteries.[22]

1.2 Lithium Sulfur Batteries

Lithium sulfur battery is one of most promising candidate for cathode materials due to high capacity, low cost and good safety performance. It is also the main topic in this thesis. I will discuss lithium sulfur batteries with principle, challenge and recent progress in this chapter.

1.2.1 Principle of Lithium-Sulfur Batteries

A lithium sulfur battery is an energy storage system that electric energy can be stored in sulfur cathode with lithium metal anode as a counter electrode. The energy will release and regain from a series of electrochemical reaction from sulfur transfer to lithium sulfide. The theoretical capacity of lithium sulfur batteries is 1672 mAh/g,[23] which is 6 times higher than 274 mAh/g, the theoretical capacity of commercialized $LiCoO_2$ cathode. Also the dominated discharge platform voltage of lithium sulfur is 2.15 V, which is lower than 3.7 V of $LiCoO_2$ cathodes.[23-24] Lower operation voltage means it has a wider range of electrical application capabilities.

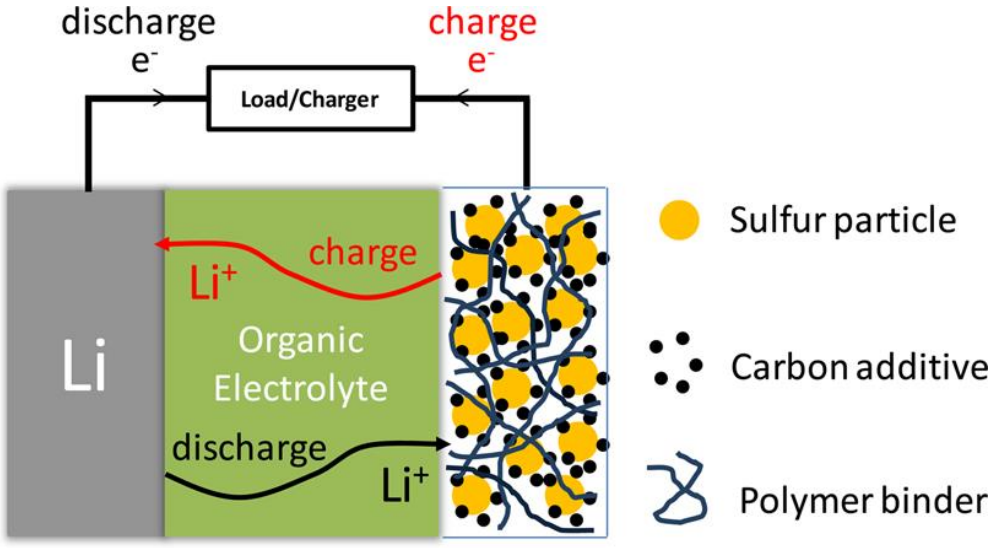

Figure 1.3 Illustrates the operation mechanism of lithium sulfur batteries.[23]

The lithium sulfur batteries system is constructed by lithium anode, organic electrolyte, and sulfur cathode. Cathode materials consist of sulfur, conductive carbon additive and polymer binder. During the electrochemical discharge process, lithium is oxidized and lithium ion transfer from lithium anode to sulfur cathode, sulfur is reduced by lithium ions to form lithium sulfide, then system generate electrons. During the charge process, sulfur in lithium sulfide is oxidized by accepting electrons and produce lithium ions and sulfur, lithium ion come back to anode and reduced when they gained electrons. The electrochemical reactions show in below:

Discharge process:

$$\text{Negative electrode: } 2Li \rightarrow 2Li^{+} + 2e^{-} \quad (5)$$

$$\text{Positive electrode: } 2Li^{+} + 2e^{-} + S \rightarrow Li_2S \quad (6)$$

Charging process:

$$\text{Positive electrode: } Li_2S \rightarrow 2Li^{+} + 2e^{-} + S \quad (7)$$

$$\text{Negative electrode: } 2Li^{+} + 2e^{-} \rightarrow 2Li \quad (8)$$

Overall net reactions:

$$2Li + S \leftrightarrow Li_2S \quad (9)$$

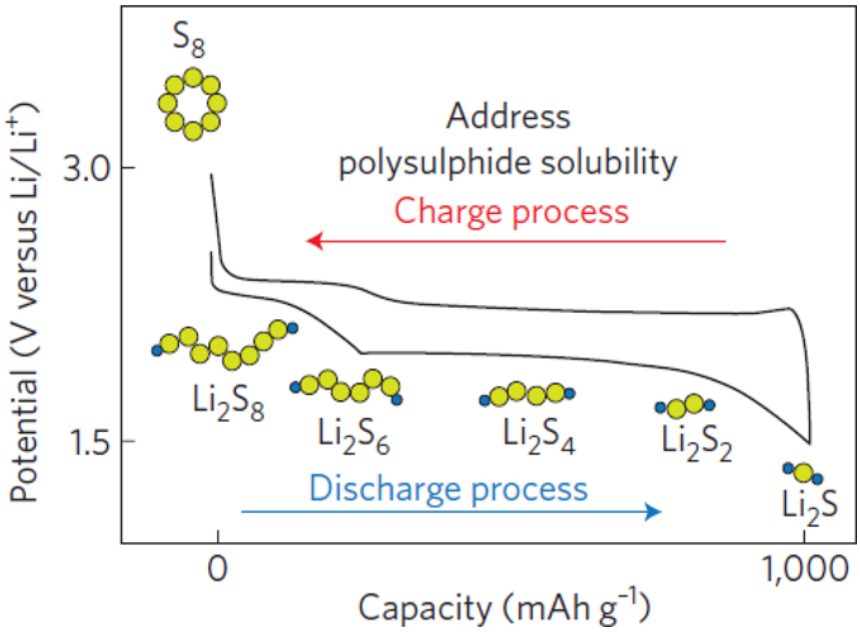

Figure 1.4 Voltage profile of Li-S battery corresponding to discharge/charge process.[23]

Sulfur atoms have a homocyclic rings with an octasulfur (S_8) molecular at room temperature. The crystal structure is orthorhombic-α octasulfur which is most stable allotrop at room temperature. During the lithium-sulfur discharge electrochemical reaction, the octasulfur is reduced by lithium ions and S_8 rings opened, results in the high-ordered lithium sulfides Li_2S_x ($6 \leq n \leq 8$) as reaction products formed first. Then reduction continues to form lower-ordered lithium polysulfides ($2 < n \leq 6$), which corresponding to the dominated discharge plateaus. At the last reaction stage, the high and lower-ordered polysulfides are reduced completely to form the Li_2S_2 and Li_2S. Respectively, the charge process also follows the same orders of polysulfides reaction with opposite direction.

1.2.2 Challenge of Lithium Sulfur

There are several technical challenges for lithium sulfur batteries, which are main obstacle for commercialization of lithium sulfur. The high electrical resistance, shuttle effect, self-discharge and volume expansion are major problems for lithium sulfur systems. These issues results in short cyclic performance, low columbic efficiency and low stability of batteries operations.

The low electrical conductivity of sulfur ($\sim 10^{-30}$ S/cm), Li_2S_2 and Li_2S is the first and important disadvantage. The electrons are not easy to be delivered to the active materials. When sulfur completely reduced to Li_2S, the Li_2S is also not easy to release the electrons to current collectors. To overcome low electrical conductivity, the uniform surrounded conductive carbon or conductive additive is the best solution. So a typical lithium sulfur system has the lower specific capacity and volumetric capacity than theoretical one.

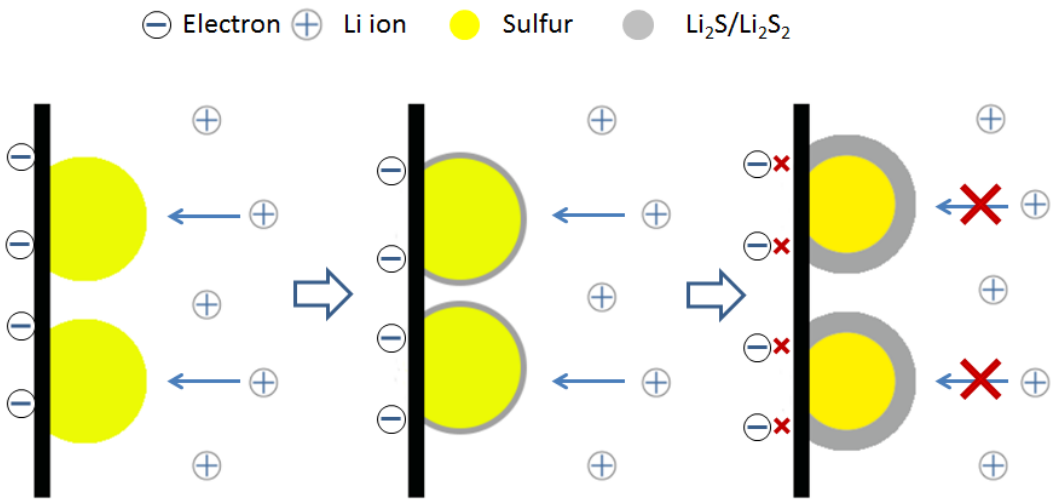

Figure 1.5 Li_2S_2 and Li_2S layer covered at surface of sulfur particles, resulting in utilization of sulfur less than 100%.

Besides, the low lithium ionic conductivity of Li_2S_2 and Li_2S is another challenge for lithium sulfur systems. When sulfur in surface of sulfur particles transform to Li_2S_2 and Li_2S, Li_2S_2 and Li_2S completely covered the sulfur particles. Sulfur in the center of the particles cannot continue to engage with the lithium-ion. So the residual sulfur can't participate in electrochemical reaction. So the actual utilization of sulfur is lower than theoretical utilization. This also is a major problem for caused by conductivity of lithium sulfur batteries.

The toughest challenge and also get most attention challenge is shuttle effect in lithium sulfur batteries. The high dissolution of high-ordered lithium polysulfides in liquid electrolyte induced freely immigration called shuttle effect. According to the illustration from figure.10 shows three regions in lithium sulfur discharge process. The transformation process from octasulfur to high ordered intermediate redox Li_2S_6 is called upper plateau region, Li_2S_6 to Li_2S_4 called slopping region, Li_2S_4 to Li_2S called lower plateau region. The high-ordered polysulfides $Li_2S_x(4\leq x<8)$ have high solubility in conventional liquid electrolyte. The low plateau region has a high reversible low ordered polysulfides shuttle, so the dissolution of them can be ignored. The dissolution of high-ordered polysulfides is the major reason for loss of sulfur and loss of capacity during cycling of batteries. It is also the major reason for low columbic efficiency of lithium sulfur batteries. To overcome shuttle effect, the several strategies based on electrolyte and protected morphology of sulfur cathode was investigated by researchers. HNO_3 is a most common additive for lithium sulfur electrolyte due to its passivation of lithium anode. It has ability to enhance the columbic efficiency by protect lithium anode erosion from shuttled polysulfide and weakened dissolved trend.[25] Also, the designing with protection layer for sulfur particles is also a solution for prevent shuttle effect. The coated protection layer has good lithium ion conductivity with low polysulfide diffusivity can effectively reduce shuttle effect.

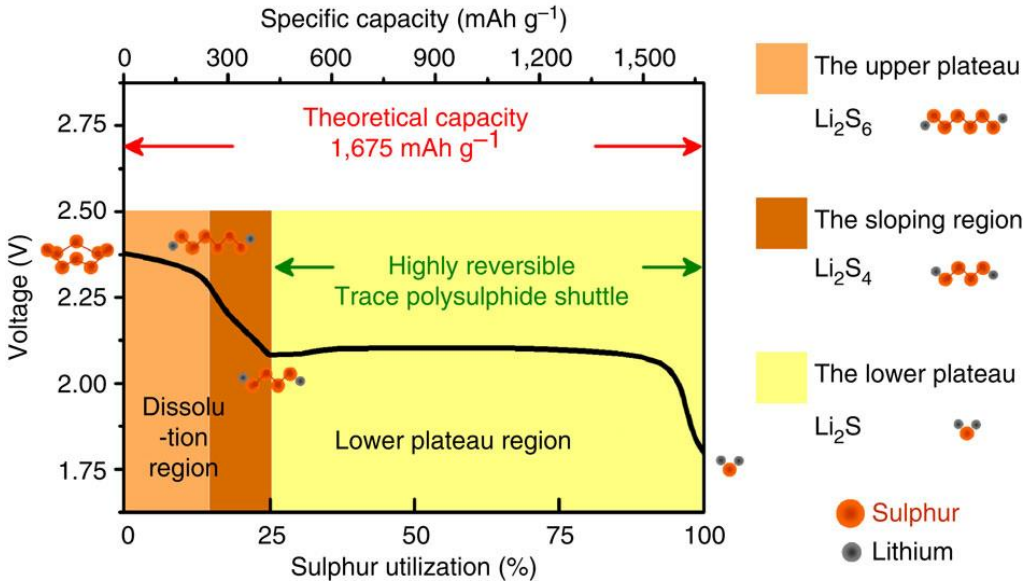

Figure 1.6. illustration discharge profiles for high-order polysulfides and low-ordered polysulfides transformations.[26]

Other challenges like volume expansion and self-discharge also are major barrier for lithium sulfur batteries need to be overcome. Self-discharge is a shuttle effect induced phenomenon for lithium sulfur batteries due to inevitable dissolution of sulfur and polysulfide even when battery is resting. Sulfur has 80% volume expansion during lithiation and delithiation, the structure fragmentation will lost conductive additive contact with sulfur, and then capacity fading will occur.

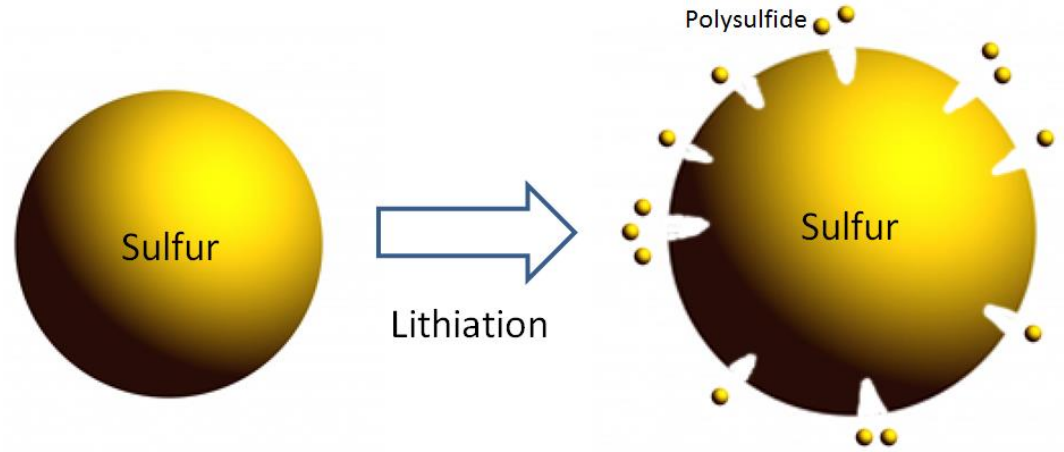

Figure 1.7 Volume expansion of lithium sulfur batteries.

1.2.3 Lithium Sulfur Progress

The prototype of lithium sulfur batteries ware investigated more than 30 years. The conductive additive and elimination of shuttle effect always are major research direction of scientists. Carbon as a low weight conductive element is a perfect conductive additive option for lithium sulfur researchers. There are many different types of carbon sulfur composites researches. In this thesis, we are committed to use the simplest form of conductive carbon blacks to design sulfur carbon composites. Various forms of carbon have a wide range of applications, such as conductive carbon blacks, porous carbons and graphene. Beside, conductive polymer additive, ceramic coating layers also have a positive effect in sulfur cathode. We will have literature reviews of recent progress in lithium sulfur batteries.

Conductive carbon blacks are widely used conductive additive materials not only for lithium sulfur, but also for almost every kind of lithium ion batteries. It is good selection with advantages of low cost and scalable synthesis materials for industries manufactory. Niu et al.[27] designed a scalable sulfur nanosponge cathode based on open network conductive carbon blacks substrate. The sulfur infused conductive carbon blacks nanosponge allow liquid electrolyte to infiltrate and enhance the lithium ion conductivity. The nanosponge structure can accommodate the volume expansion during lithiation process. Respectively, the conductive carbon blacks will spontaneously form a passivation layer to slow down the shuttle effect. Ji et al.[24] reported a precisely controlled sulfur growth inside the channel of conductive mesoporous carbon framework. The conductive mesoporous carbon structure provides a sufficient contact with insulating sulfur and structure also effectively trapped polysulfides during electrochemical reaction. Chen et al.[28] reported monodispersed sulfur nanoparticles at reduced graphene oxide composites perform the theoretical discharging/charging capacity at first cycle at 0.1C

discharging/charging rates. They use EDA-S precursor to grow the sulfur nanoparticles at reduced graphene oxide sheet, and 5 nm average size and uniformly distribution sulfur particles gained in their batteries performance.

They can precisely control their particles size by modifying the reaction conditions. They also proved the smaller sulfur particles size can close the theoretical capacity in lithium sulfur batteries. Meanwhile, they claimed the 5nm sulfur particles size can completely avoid the insulating blocking the lithium ions transfer by Li_2S_2 and Li_2S. Excellent electrical conductivity performance of graphene is a promising candidate for the conductive additive in lithium sulfur batteries. Seh et al.[29] report a sulfur-TiO_2 yolk shell nanostructure deliver an protect shell with internal void to accommodate the volume expansion. The TiO_2 yolk shell can minimize the loss of polysulfides and will not crack due to void to accommodate the volume expansion. The coulombic efficiency remained 98.4% and capacity decay less than 0.033% per cycle after 1000 cycles. The good performance with long cycle lithium sulfur batteries is a gained in this works.

2. Experimental

2.1. Materials

Materials used for the experiments are listed in Table 1.

Materials	Vendor	Chemical formula
Sulfur	Sigma	S_8
Ethylenediamine	Sigma	$C_2H_4(NH_2)_2$
Hydrochloric acid	Alfa Aesar	HCl
Carbon black (Super P)	Timcal	C
Separator		PP/PE/PP
Nitric acid	Alfa Aesar	HNO_3
Electrolyte		1M LiTFSI in DOL and DME
Lithium nitrate	Alfa Aesar	$LiNO_3$
Active charcoal	Sigma	C

Table 1 Main materials used in experiments.

2.2 Synthesis of Materials

EDA-S Precursor Based Carbon-Sulfur Composites

50 mg sulfur and 2.5ml Ethylenediamine (EDA) were added into a vial, then sonicated and stirred until sulfur dissolved in EDA (dissolution reaction: $2(R–NH_2) + S_8 \rightarrow (R–NH_3^+)(RNH–S_8)^-$), the dark red EDA-S precursor (Show in Figure 5a) formed. Meanwhile, 21 mg Carbon Blacks are sonicated in 60 ml 1M HCl for 1 hour inside the three-necked flask. After carbon blacks were well dispersed in HCl solution, high purity argon was passed into flask to protect reaction environment (the aim for argon gas is to avoid reaction $H_2NCH_2CH_2NH_2 + CO_2 + H_2O \rightarrow H_2NCH_2CH_2NH_3HCO_3$ occurred and reaction setup is shown in Figure 5b). Then EDA-S precursor was dropped into HCl-C solution with drop speed 1ml/min. Then both solution reacted

5 minutes under 600 rpm magnetic stirring and argon gas protection until the solution became transparent from yellow-green.

$$(R–NH_3)^+(RNH–S_8)^- + 2H^+ \rightarrow 2(R–NH_3)^+ + S_8 \downarrow \quad (10)$$

S-Carbon blacks synthesis composites are based on reaction (10). Our goal is to control the reaction parameters to control sulfur particles size. Finally, reaction product were filtered and rinsed by DI water and dried in vacuum oven at 70°C for 24 hours.

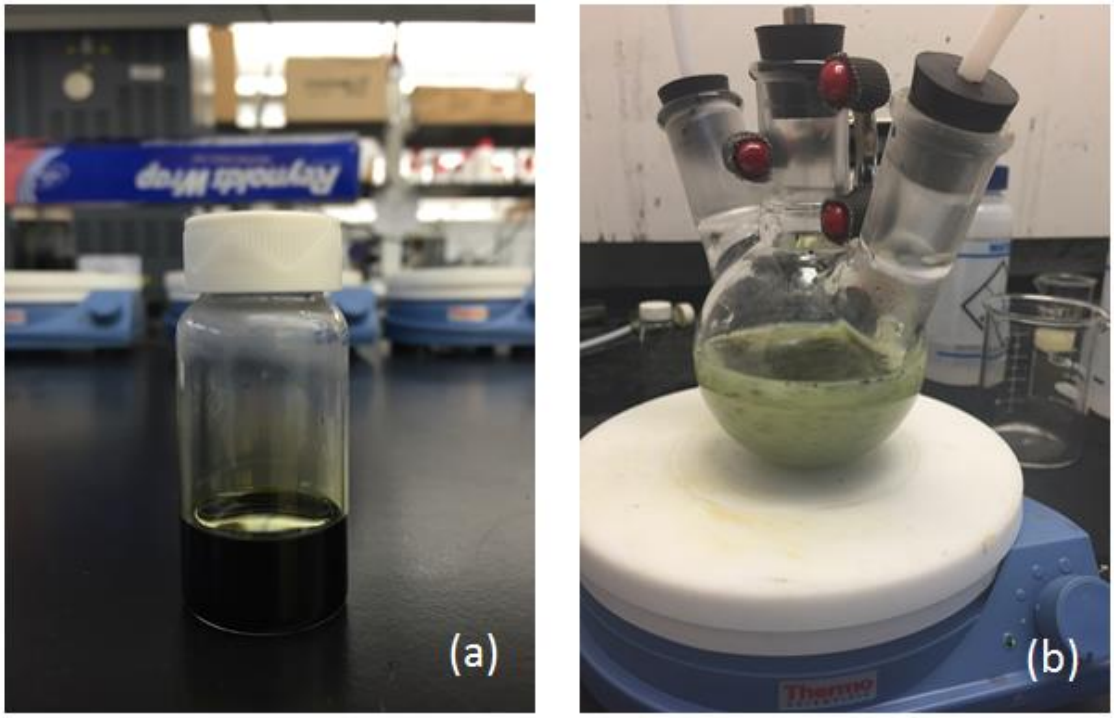

Figure 2.1(a) Dark red EDA-S precursor, (b) Three-necked flask reaction setup.

Nanosponge Carbon-Sulfur Composits

70mg Sulfur and 30mg conductive carbon blacks were mixed with mortar milling for 20mins. And 100mg S-C mixture heat treated at 200°C for 2.5 hours inside quartz tube of furnace. Argon purged in as a protective gas with speed of 100ppm. Sulfur Carbon electrode materials were cooled down inside furnace. Nanosponge carbon-sulfur composites were prepared.

Acid Treated Nanosponge Carbon-Sulfur Composites

500mg conductive carbon blacks were treated with 10%HF for 6 hours. Then carbon blacks were treated 80% HNO_3 at 80°C inside flask with oil bath for 15 hours. Treated carbon blacks were filtered and rinsed using DI water and ethanol. The weight ratio of sulfur: treated carbon blacks = 7:3 are heat treated at 155°C in muffle furnace for 15 hours. And same ratio sulfur and carbon heat treated at 200°C for 2.5 hours inside quartz tube of furnace. After heat treatment, sulfur is 68.5 wt% (at 155°C for 8 h) and 66.2 wt% (at 200°C for 2.5 h), respectively.

2.3 Battery Assembly

The carbon-sulfur composites materials, carbon blacks, binder PVDF were mixed with weight ratio of 8:1:1 to form electrode materials. The mixtures were grinded in mortar milling for 20 minutes and then N-Methyl-2-pyrrolidone (NMP) liquid were added into electrode materials. And electrode slurry was uniformly dispersed under magnetic stirring for 2 hours and sonicated for 1 hour. Then slurry was uniformly coated on aluminum foil with 1.5 mg/cm^2 active materials loading ratio. Then slurry coated Al foil was dried at 70°C under vacuum oven for 24 hours. Then dried slurry foil was pressed by hydraulic Press machine with 2 tons for 2 hours, and was sliced by cutting machine for battery assembly. The sulfur carbon composites cathode is prepared. Since lithium-sulfur has especially electrochemical reaction mechanism we have

described in Introduction 2.1. In order to avoid the dissolution of intermediate polysulfide, we use 1:1 volume ratio 1,3-dioxolane (DOL) and dimethoxyethane (DME) and 1M bis(trifluoromethane)sulfonamide (LiTFSI) lithium salt and 2wt% $LiNO_3$ solution as our electrolyte.

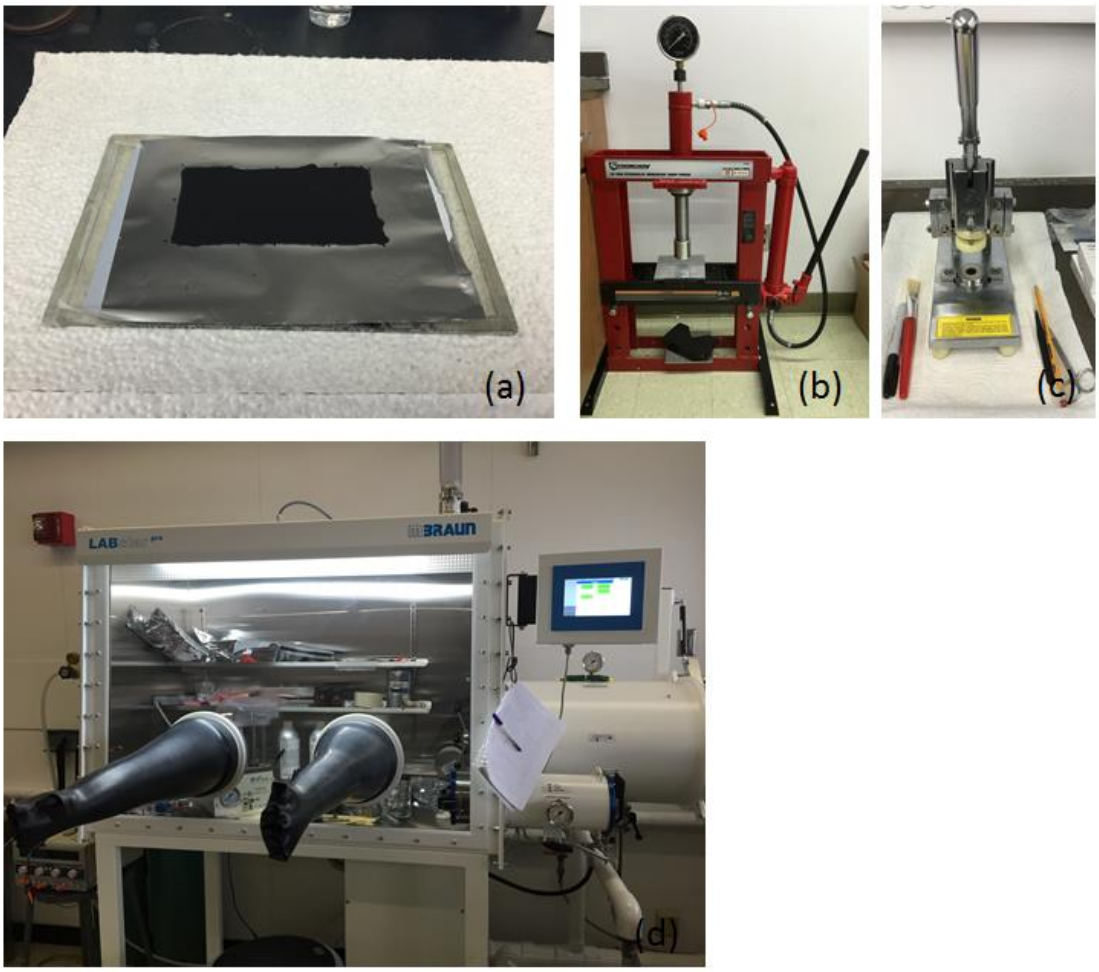

Figure 2.2 (a) Slurry coated aluminum foil, (b) (c) Hydraulic press and cutting tools. (d) Argon filled MBraun LABstar glove box workstation.

Coin cell was assembled inside MBraun LABstar glove box workstation at argon filled environment with H_2O content less than 0.5 ppm. The assembled sequence is stainless steel spring, stainless steel spacer, and cathode, and separator, disc lithium slice with sufficient electrolyte (1M LiTFSI in DOL/DME by volume ratio 1/1 and 2 wt% $LiNO_3$ additive).

2.4 Materials Characterization Facility

X-Ray Diffraction (XRD)

Crystal structure of carbon sulfur composites materials were analyzed by Bruker D8 Discover XRD instrument. Cu-Kα is X-Ray source with scanning range of 10-70°.

Scanning Electron Microscope (SEM)

The topography and morphology of the materials were characterized by Hitachi S-4800 SEM, and elemental distribution analysis were observed by energy-dispersive X-ray spectroscopy EDS mapping mode.

Transmission Electron Microscope (TEM)

Also Hitachi H-9000NAR high resolution TEM used for further crystal structure and morphology characterization.

Electrochemical Performance Characterization

Electrochemical charge-discharge curve and battery cyclic performance were tested by Landt Instrument Battery tester. Cyclic voltammetry is measured by Gamry electrochemical workstation Reference 600+ Potentiostat/Galvanostat/ZRA.

Figure 2.3(a) Hitachi H-9000NAR high resolution TEM, (b) Landt battery test system, (c) Gamry electrochemical workstation.

3. Results and Discussion

3.1 EDA-S Precursor Based Carbon-Sulfur Composite

3.1.1 Chemical Synthesis Analysis

Our initial plan is to reduce the sulfur particles size and get uniformly distribution sulfur particles on conductive carbon blacks substrate. Also EDA-S precursor based Carbon-Sulfur Composite need to overcome huge volume expansion; also we need to make the greatest efforts to reduce the loss of sulfur during charge/discharge process. According to literature research, we believe particle size could help improve the utilization ratio of sulfur. Since small particles size sulfur may get a more sufficient reaction ratio compare with large particle size. Larger sulfur particles can be blocked by insulation reaction intermediates Li_2S and Li_2S_2 at surface. But the smaller sulfur particles may have lower possibility to form these insulation intermediates since higher specific surface area and higher reaction rates. So the smaller particle size means sulfur cathode materials will have a specific capacity closer to their theoretical capacity. We designed a series of experiments to synthesis a uniformly sulfur carbon composites materials with smaller sulfur particles based on chemical reaction. Factors determine the sulfur particles size was studied by our comparison experiment. For instance, sulfur concentration in EDA precursor, the concentration of hydrochloric acid, drop speed of reaction, pH value of solution after reaction, reaction time and reaction environments. We hope that by adjusting these factors can control the reaction kinetics, thereby obtaining uniformly distribution nano sulfur particles in our sulfur carbon composites. We suspect that the more dilute reaction solution and the slower drop speed can help to have slower reaction environment from reaction kinetics.

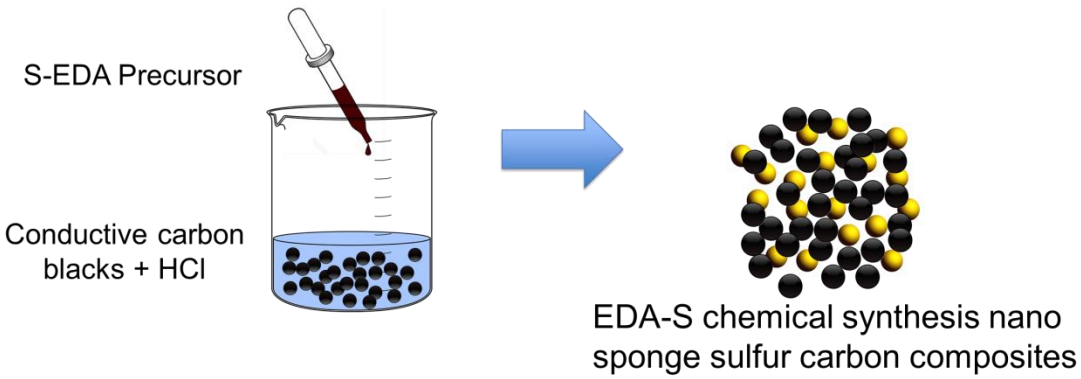

Figure 3.1 Reaction mechanism of EDA-S carbon composites.

Factors / Results	S	EDA	Concentrati-on of S-EDA	C	HCl	HCl concentr-ation	Total reaction time	Reaction Environme-nt	pH	Drop Speed
1-8 µm S	300 mg	2.5ml	3.75mol/L	126mg	60ml	1N	7.5 min	Stirring	7	1ml/min
1-5µm S	100 mg	2.5ml	1.25mol/L	42mg	60ml	1N	7.5 min	Stirring	7	1ml/min
0.5-2 µm S	50 mg	2.5ml	0.625mol/L	21mg	60ml	1N	7.5 min	Stirring	7	1ml/min
1-5 µm S	50 mg	5 ml	0.3125mol/L	21mg	120ml	1N	10 min	Stirring	7	1ml/min
0.5-2 µm S	50 mg	2.5ml	0.625mol/L	21mg	60ml	1N	7.5 min	Stirring	7	1ml/min
1-5 µm S	50 mg	2.5 ml	0.625mol/L	21mg	60ml+ 100ml H_2O	0.375mol/L	7.5 min	Stirring	7	1ml/min
1-2 µm S	50 mg	2.5ml	0.625mol/L	21mg	60ml HCl +540 ml H_2O	0.1mol/L	7.5	Stirring	6-7	1ml/min
No S	50 mg	2.5 ml	0.625mol/L	21mg	75 ml	1N	7.5 min	Stirring	1	1ml/min
1-3 µm rare S	50 mg	2.5 ml	0.625mol/L	21mg	65ml	1N	7.5 min	Stirring	3	1ml/min
No S	50 mg	2.5 ml	0.625mol/L	21mg	55ml	1N	7.5 min	Stirring	10	1ml/min
No S	50 mg	2.5 ml	0.625mol/L	21mg	20ml	1N	7.5 min	Stirring	14	1ml/min
No S	50 mg	2.5 ml	0.625mol/L	21mg	60ml	1N	17 min	Stirring	7	5 drop/min
5 µm S	5mg	2.5ml	0.625 mol/L	21mg	60ml	1N	5 min	Stirring	7	1 min All drop
No S	50 mg	2.5 ml	0.625mol/L	21mg	60ml	1N	120 min	Stirring	7	1 drop/5min
500 nm	50 mg	2.5ml	0.625mol/L	21mg	60ml	1N	7.5 min	Stirring at Ar protection environment	7	1ml/min

Table 2 Main factors versus sulfur particles size.

Through this series experiment, sulfur particles precipitated at surface of conductive carbon blacks template which in EDA-S precursor and HCl reaction solution. Using TEM characterization techniques to observe particle size, we adjusted our experimental strategies step by step. We successfully reduced sulfur particles size from the micron level to 500 nm. We found the most appropriate EDA-S concentration is 0.625mol/L, the reaction solution60 ml 1 mole/L HCl. Also, we found pH value is critical parameters for precipitating sulfur particles. In acidic solutions with pH value of 1, we didn't get the sulfur particles, and when pH value is 3 with rare sulfur precipitation. On the other hand, alkaline solution had no any sulfur particles observed. We observed light yellow suspension precipitated inside the reaction solution and it fade away quickly to yellow-green transparent solution. The phenomenon gives us an intuitive explanation of sulfur precipitation first and quickly dissolved again in solution.

3.1.2 XRD Results

XRD patterns of EDA-S carbon composites have clearly peaks correspond to standard orthorhombic Sulfur peaks. Figure for XRD patterns indexed (111), (113), (222), (026) and (311) planes of orthorhombic sulfur. From point views of sharp peaks, the chemically synthesized sulfur has good crystallinity. And conductive carbon blacks can't be detected due to the amorphous structure.

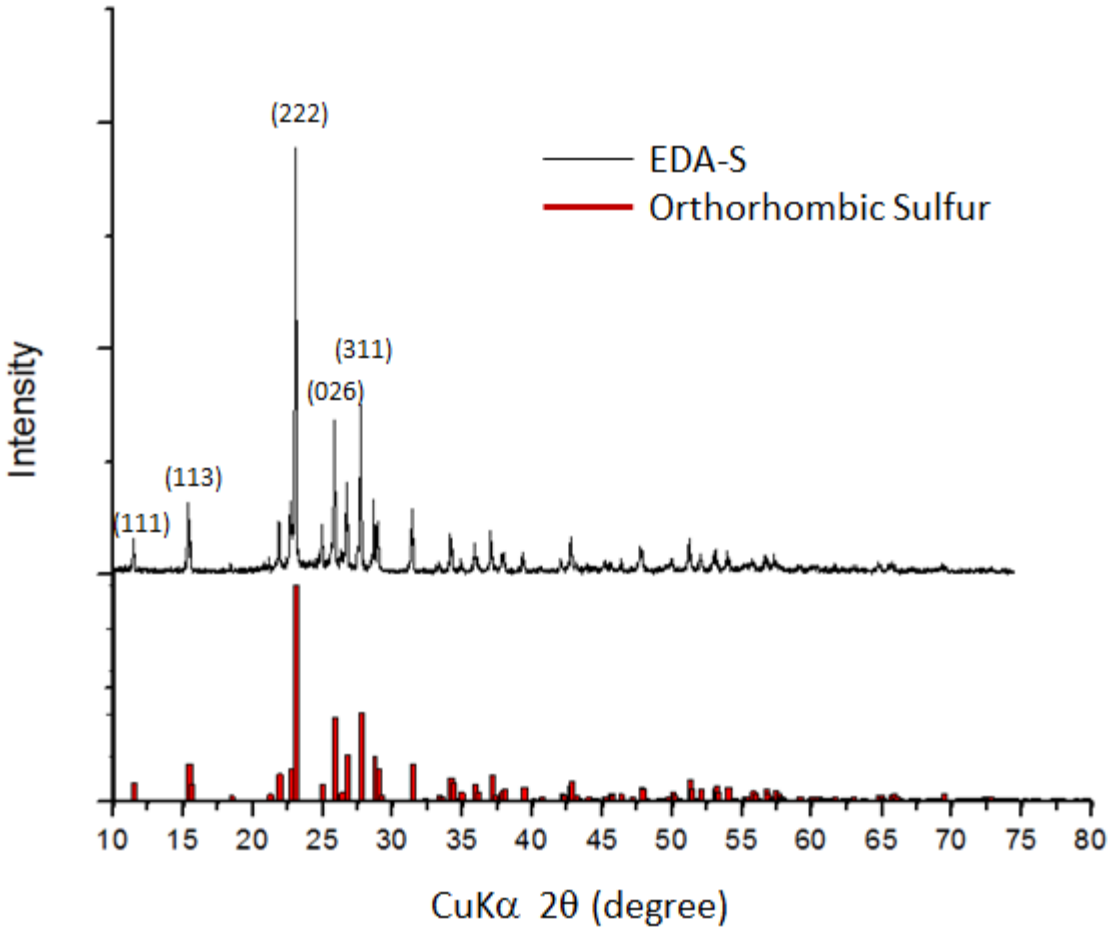

Figure 3.2 XRD pattern shows orthorhombic sulfur of EDA-S.

3.1.3 TEM Analysis

TEM images show in below are morphology of our sulfur-carbon composites. Sulfur is beam sensitive materials because sulfur is insulation materials with low melting point of 115°C. When electron beams incident to samples, electrons are easier to aggregate at surface of sulfur, and sufficient electron resource will cause strong vibrations at surface. The temperature will increased from energy of vibration, when temperature reached to melting point, the liquid sulfur will be pumped from high vacuum environment of TEM chamber. So we can only observe the sulfur particles at low magnification.

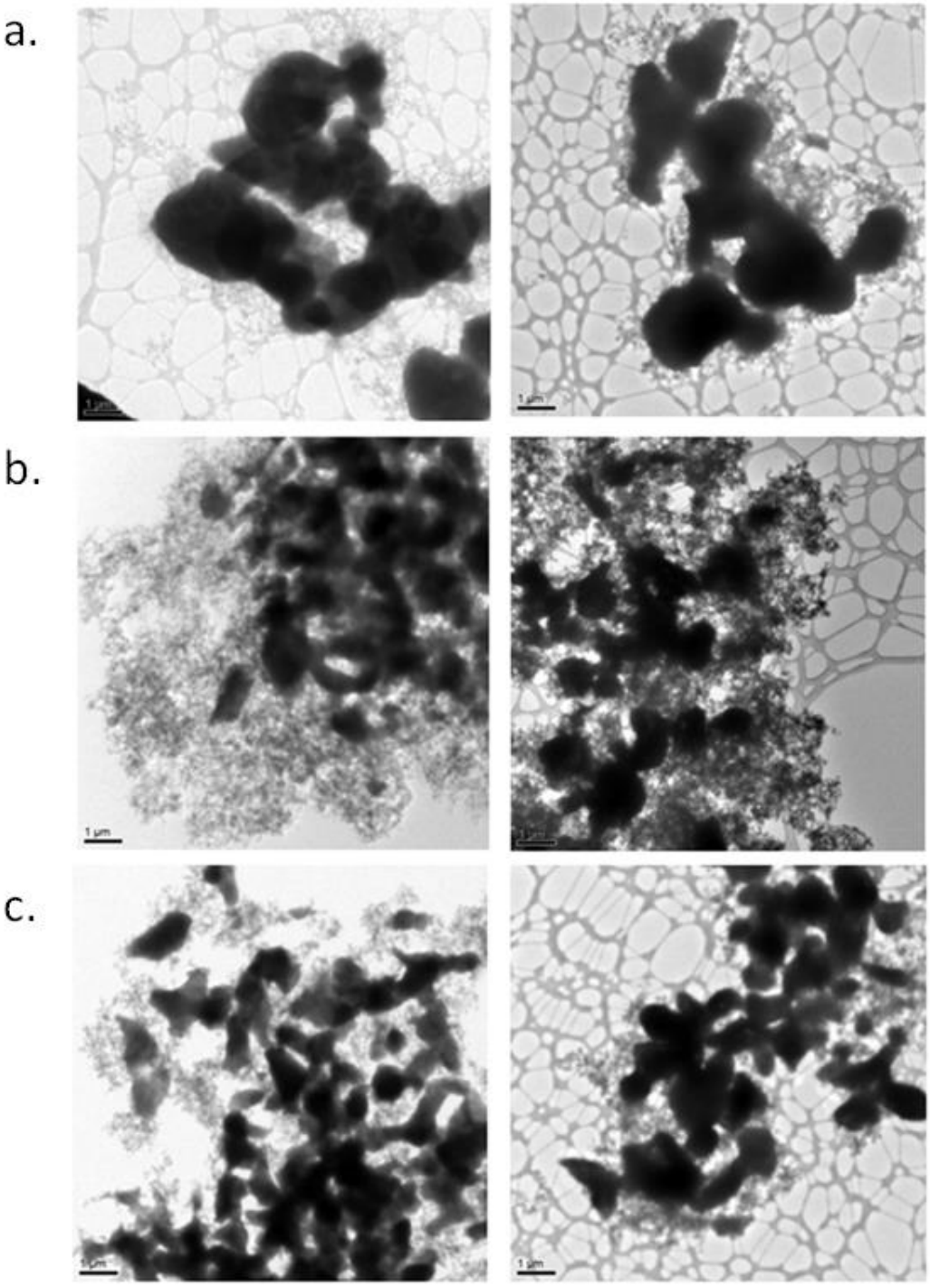

Figure 3.3. (a) Average particles size with 1 to 8μm at 3.75 mol/L S concentration in EDA, 60mL 1N HCl, reaction time 7.5 min at air stirring environment, pH value 7 and drop speed 1mL/min. (b). Average particles size with 1 to 5μm at 1.25 mol/L S concentration in EDA. (c) Average particles size with 500nm to 1 μm at 0.625 mol/L S concentration in EDA at argon protected reaction environment.

From our TEM images, we can observe the uniform distribution of sulfur particles at conductive carbon blacks substrate. Also we found the trend to reduce the sulfur particles size via control the several reaction parameters. The major factor is sulfur concentration in EDA precursor, we found the lower concentration can provide a mild sulfur precipitation kinetic process, so the smaller sulfur particles size we can synthesis. The HCl concentration is a factor can determine the homogeneous or heterogeneous nucleation of sulfur particles. We glad to see homogeneous sulfur particles nucleation during reaction. The pH value of solution after all drops also is a critical factor to get sulfur particles, which is highly related to the amount of HCl. 20% amount of HCl less than theoretical neutralization amount is also the experimental phenomenon we could control the pH value remain on 7. Besides, argon protection reaction environment eliminate the adverse effects of carbon dioxide and water in air.

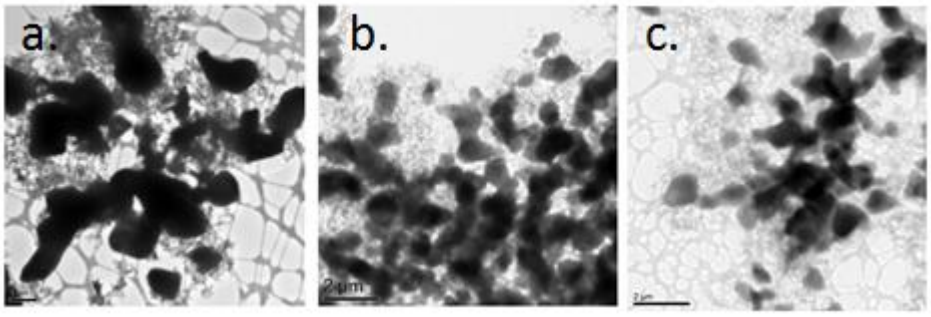

Figure 3.4 (a), Average particles size with 1 to 5μm at 0.1M HCl reaction solution (b), average particles size with 0.5 to 2μm at 0.5M HCl reaction solution (c), average particles size with 0.5 to 1μm at 1M HCl reaction solution.

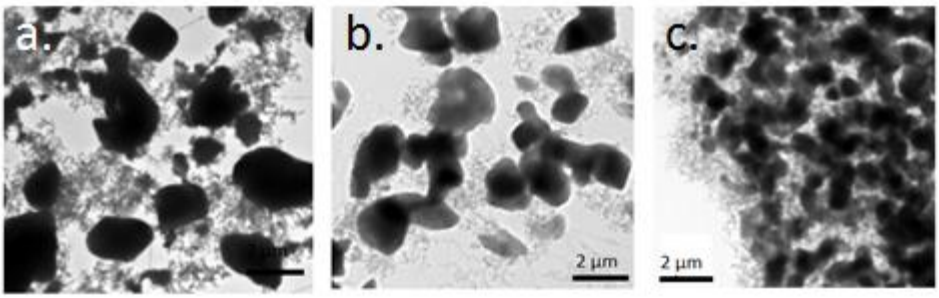

Figure 3.5 (a), Average particles size with 1 to 5μm at 2.5 ml/min drop speed (b), average particles size with 0.5 to 5μm at 0.2 ml/min drop speed (c), average particles size with 0.5 to 1μm at 1 ml/min drop speed.

3.1.4 SEM Analysis

SEM images of EDA-sulfur carbon composites demonstrated the distinct sulfur particles surrounded by conductive carbon blacks. The sphere particles are sulfur and floc materials on sulfur particles is network of conductive carbon blacks. The network of conductive carbon blacks is able to deliver an electrical conductivity connection. The network also can provide partial protection for avoiding loss of polysulfide. There are enough interspaces among each sulfur particles, which can accommodate the volume expansion.

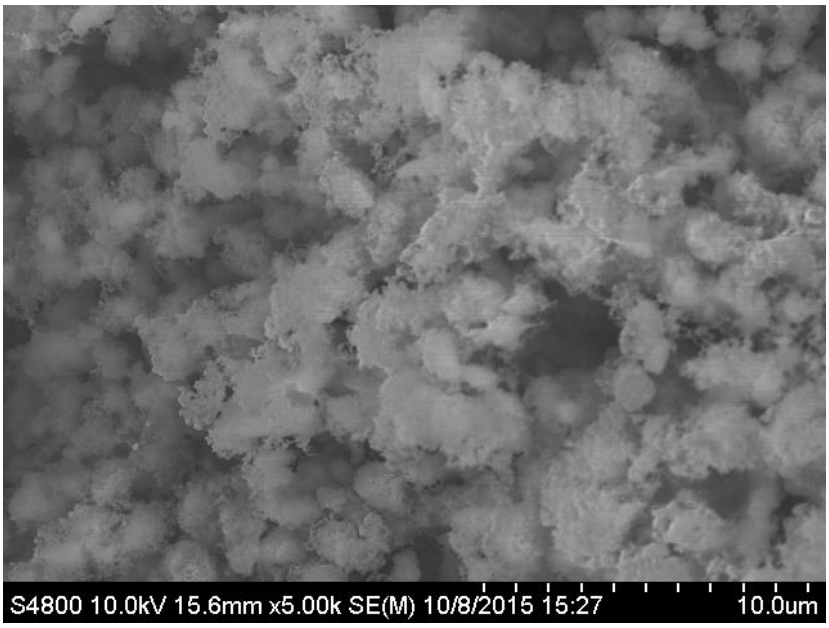

Figure 3.6 Morphology of EDA-S carbon composites characterized by SEM.

The Energy dispersive X-ray spectroscopy (EDS) mapping proved the uniform distribution of sulfur particles. Also the EDS mapping of carbon shows not uniformly distribution, only get signals from detector closer side. Carbon only has characteristic X-ray from K-shell electron excitation; sulfur has characteristic X-ray from K-shell and L-shell. The sulfur has stronger signal detected than carbon, and also the characteristic X-ray from K-shell can be absorbed by sulfur particles too. These are reason for non-uniform distribution for carbon EDS mapping.

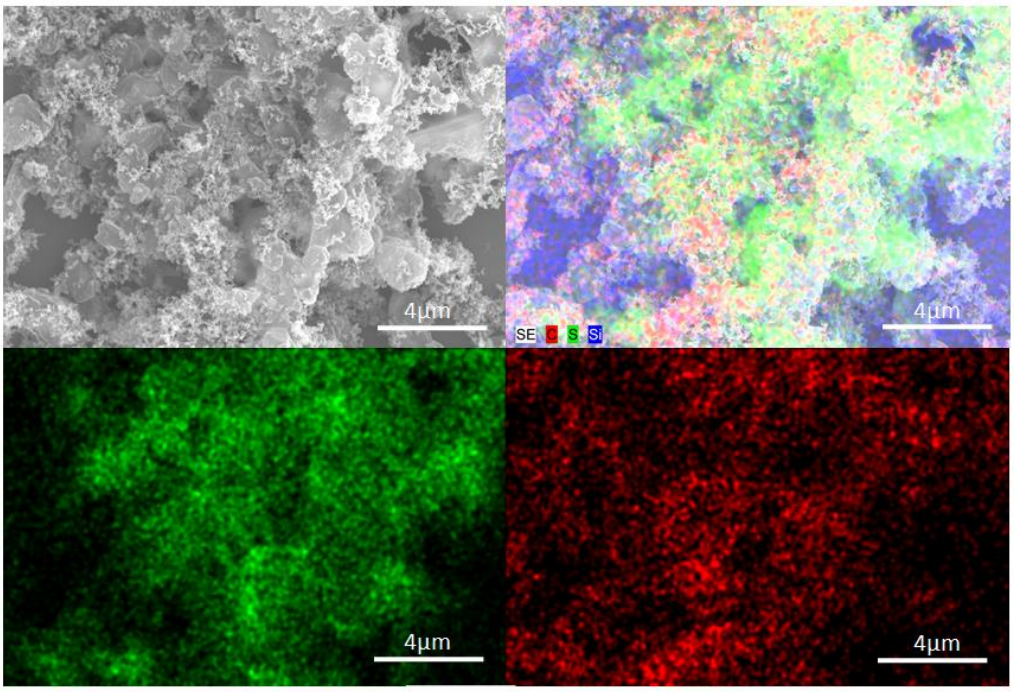

Figure 3.7 EDS mapping of EDA-S carbon composites.

3.1.5 Cyclic Voltammetry

Shown in Figure 20 is the cyclic voltammetry profile at a scanning rate of 0.01 mV/s. Two inverted peaks in the bottom were observed during lithiation/discharging process, corresponding to two reduction process in sulfur cathode. The first peak at range of 2.30-2.35V indicate reduction product of high-ordered lithium polysulfide (Li_2S_n, $4 \leq n < 8$) of earlier stage electrochemical reaction between lithium and sulfur. The second peaks at 2.05V correspond to low ordered lithium polysulfide (Li_2S_2, Li_2S), that high-ordered lithium sulfides to low-ordered lithium sulfide transformation occurs in further reaction stage. Parallel, the two oxidation process of cathode also occurred at 2.30V and 2.38V, indicating that charge process occurred transformation from Li_2S/ Li_2S_2 to Li_2S_n ($4 \leq n \leq 8$) and Li_2S_n ($4 \leq n \leq 8$) to S_8.

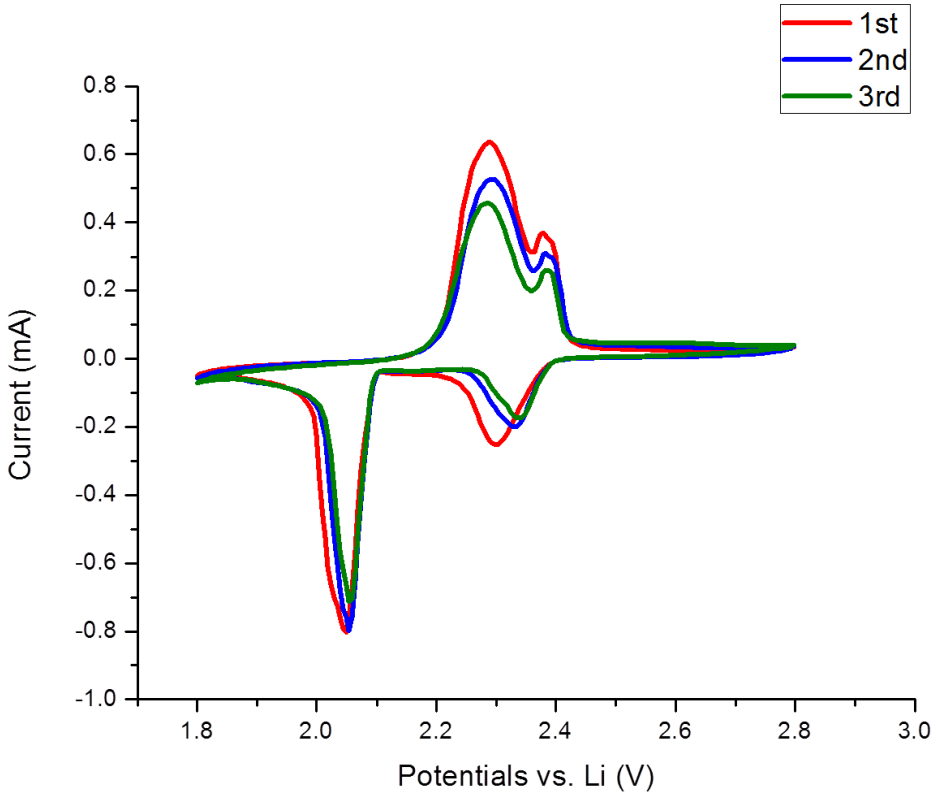

Figure 3.8 CV curves of synthesized EDA-S carbon composites lithium sulfur batteries.

Furthermore, we can observe the second cycle and third cycle have apparent position shift and peak current decrease. The slightly over-potential in first cathodic reduction peak is caused by favorable sulfur-carbon interface have not formed yet. After initial cycle, the over potential disappeared possibly due to rearrangement of active materials. The materials structure slightly changed to its electrochemical natural tendency. Also, the current density decrease means loss of active materials. This phenomenon cause by shuttling effect induced sulfur loss.

3.1.6 Cyclic Performance

The specific capacity of our EDA sulfur carbon composites in first discharge cycle is 1032 mAh/g, and second cycle discharge capacity is 962mAh/g with coulombic efficiency of 94% at 0.2 C discharge/charge rate. The two discharge plateaus in first cycle obviously distinct in 2.25V and 1.95 V. The upper plateau corresponding to S_8 to Li_2S_6 is short and slopping region has a pretty fast degradation rate. And lower plateau has a long and stable performance, which can provide a regulated power output. Possibly, our crystal sulfur particles have a high efficiency on the electrochemical kinetics. So it has a fast reduction reaction in high-order polysulfide transform to low-order polysulfide process. And sulfur utilization in lower plateau is about 70%. At first three charge cycle, the two plateaus are around 2.3V and 2.45V, which correspond to delithiation process of Li_2S to Li_2S_4 and Li_2S_4 to S_8. The charge curve is flat at beginning stage without bumps, it prove no obvious SEI layer formation.

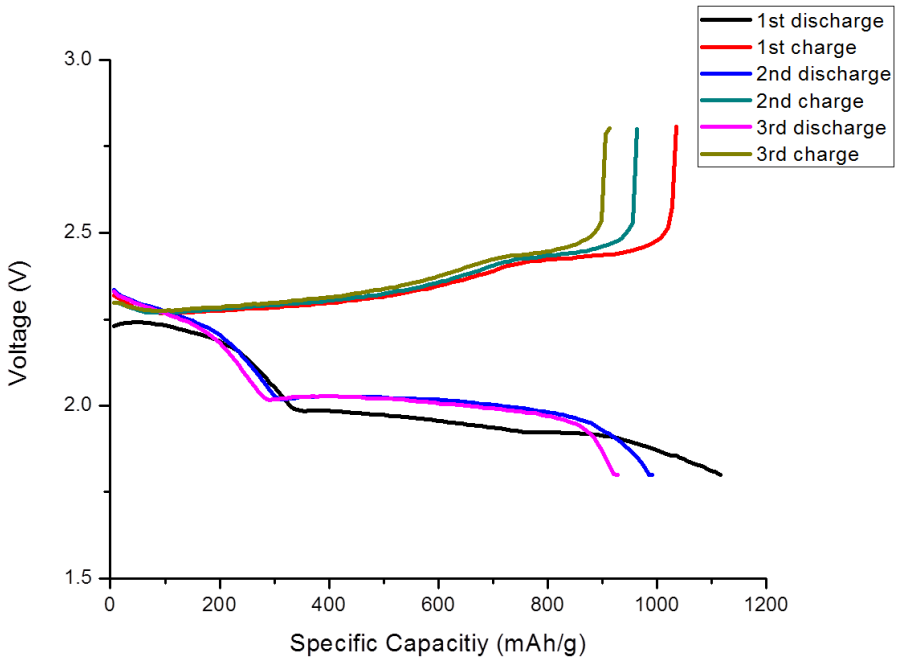

Figure 3.9 First 3 cycles discharging/charging curves of synthesized EDA-S carbon composites lithium sulfur batteries at 0.2C.

From Figure 20, the initial capacity starts from 1032 mAh/g and coulombic efficiency of 94%. Also we can see capacity degradation rate is fast during first 50 cycles due to shuttle effect induced loss of sulfur. After 50 cycles, the loss of capacity trend slow down and coulombic efficiency slightly increases. After 100 cycles, the capacity and coulombic efficiency tend to stabilize about 200 mAh/g and 97%.

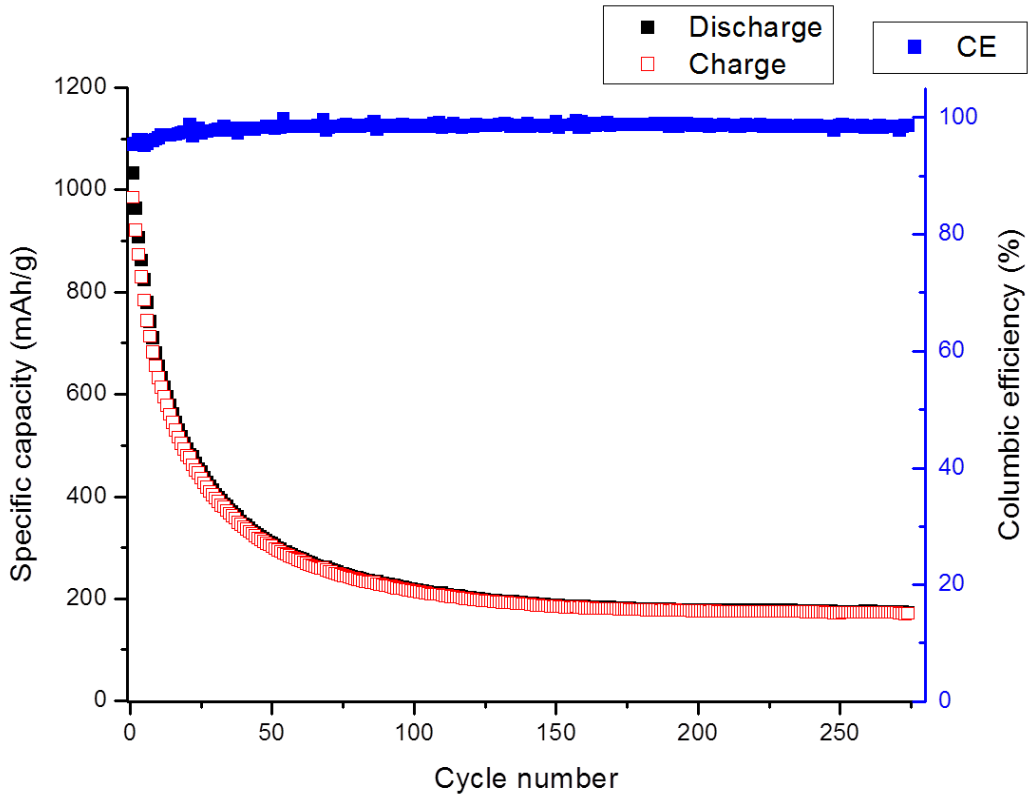

Figure 3.10 Cyclic performance and coulombic efficiency of synthesized EDA-S carbon composites lithium sulfur batteries at 0.2C.

3.2 **Nanosponge Carbon-Sulfur Composites**

Nanosponge carbon-sulfur composites is a very simple synthesis method and scalable production. We use mortar milled mixture of commercial sulfur and conductive carbon blacks as resource. Only 24 hours heat treatments at 155 °C need to be applied in synthesis. The sulfur is heated above its melting point, and fully wetted among the carbon substrate. Then, melted sulfur cooled at air. Nanosponge carbon-sulfur composites of fully adhesions on carbon synthesized.

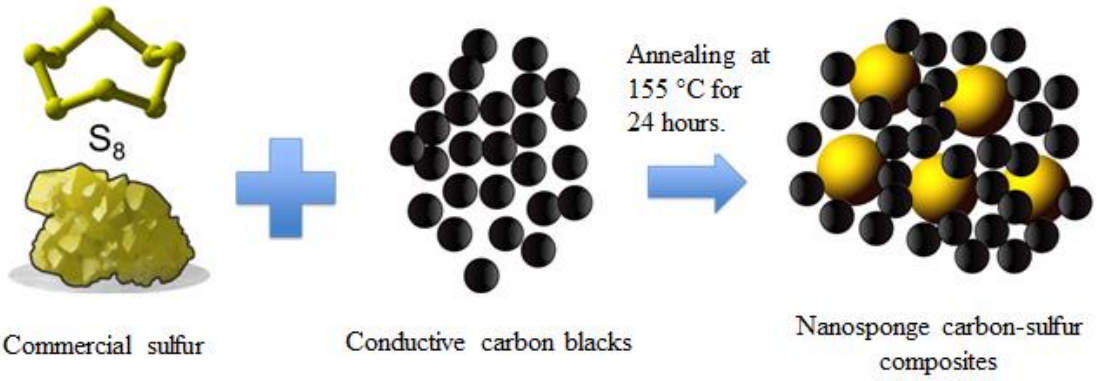

Figure 3.11 Synthesis of nanosponge sulfur carbon composites.

3.2.1 XRD Analysis

XRD pattern of nonosponge carbon-sulfur composites demonstrate a semi-crystalline state monoclinic crystal structure. Sulfur has a phase transformation at 95.4 °C, from rhombic sulfur to monoclinic sulfur. Because of cooling at air, Semi-crystalline state monoclinic crystal structure didn't have enough time to transform back to rhombic sulfur. It also has most characteristic peaks of monoclinic sulfur.

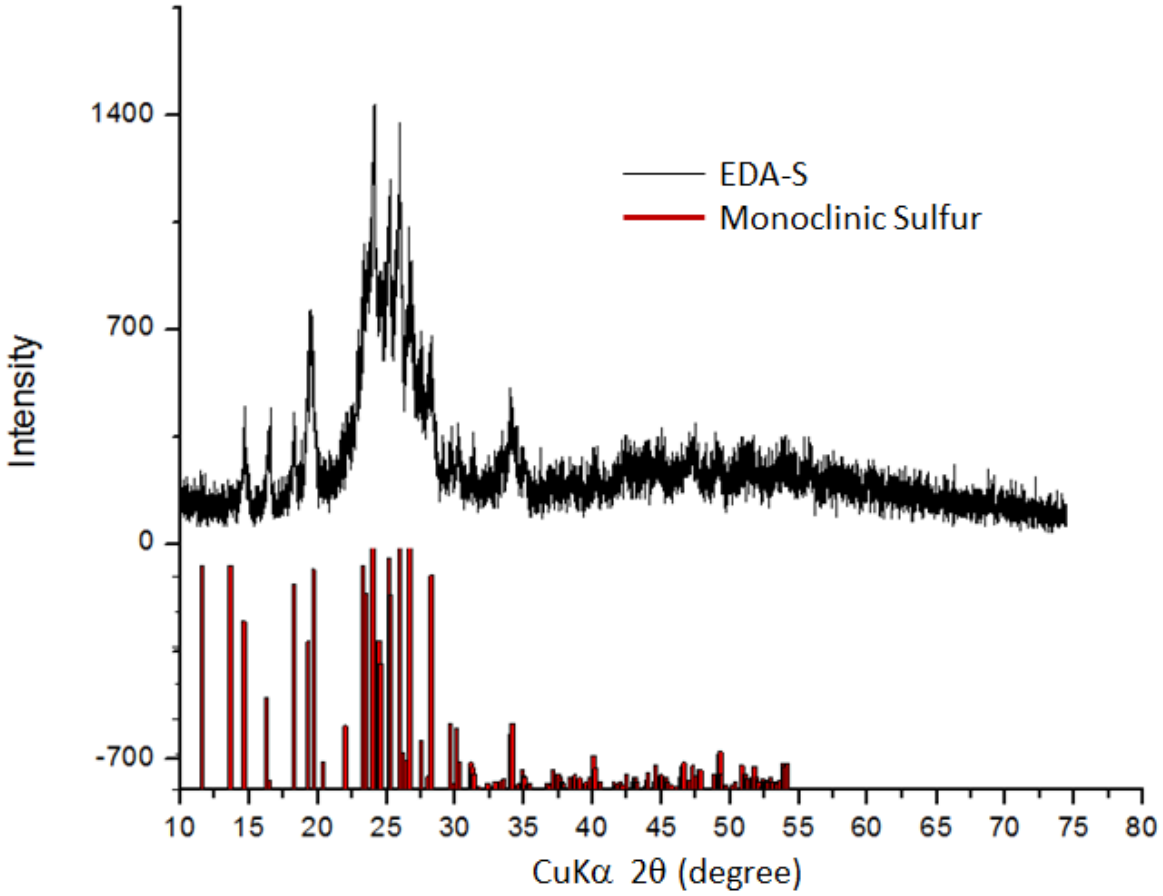

Figure 3.12 XRD pattern of nanosponge sulfur carbon composites.

3.2.2 Voltage Profile Analysis

The information from charge discharge curve shows the specific capacity of nanosponge sulfur carbon composites at first discharge cycle is 1404 mAh/g. The first cycle has an initial capacity close to theoretical capacity, since sulfur has sufficient contact with conductive carbon. The first discharge plateau is unrecognizable between 2.35V to 2.0 V. The reaction from S_8 to Li_2S_6 behave continues discharge curve. And lower plateau has a recognizable curve at 1.95 V. At first charge cycle, the mainly charge plateaus is around 2.0V, which correspond to delithiation process of Li_2S to S_8. The charge curve has a bump at beginning stage, it possibly is formation of SEI layer.

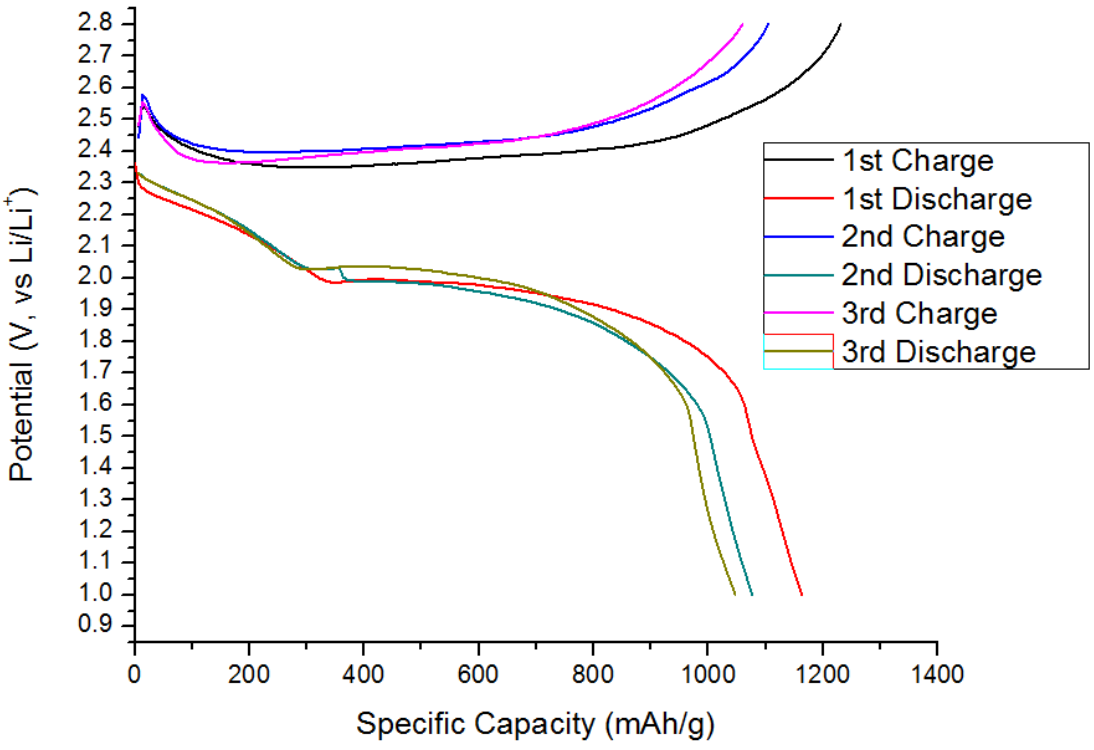

Figure 3.13 Charging/discharging curve of nanosponge sulfur carbon composite at 0.2C.

3.2.3 Cyclic Performance

From Figure 20, the initial discharge capacity starts from 1404 mAh/g at 0.2C and coulombic efficiency is 95%. At 50th cycles, the 600mAh/g remained. We can see capacity degradation rate is fast during first 50 cycles due to shuttle effect induced loss of sulfur. At 100th cycles, the capacity down to 484mAh/g, and the loss rate of capacity tend to a constant value. After 100 cycles, the capacity was still decreasing due to unavoidable shuttle effect.

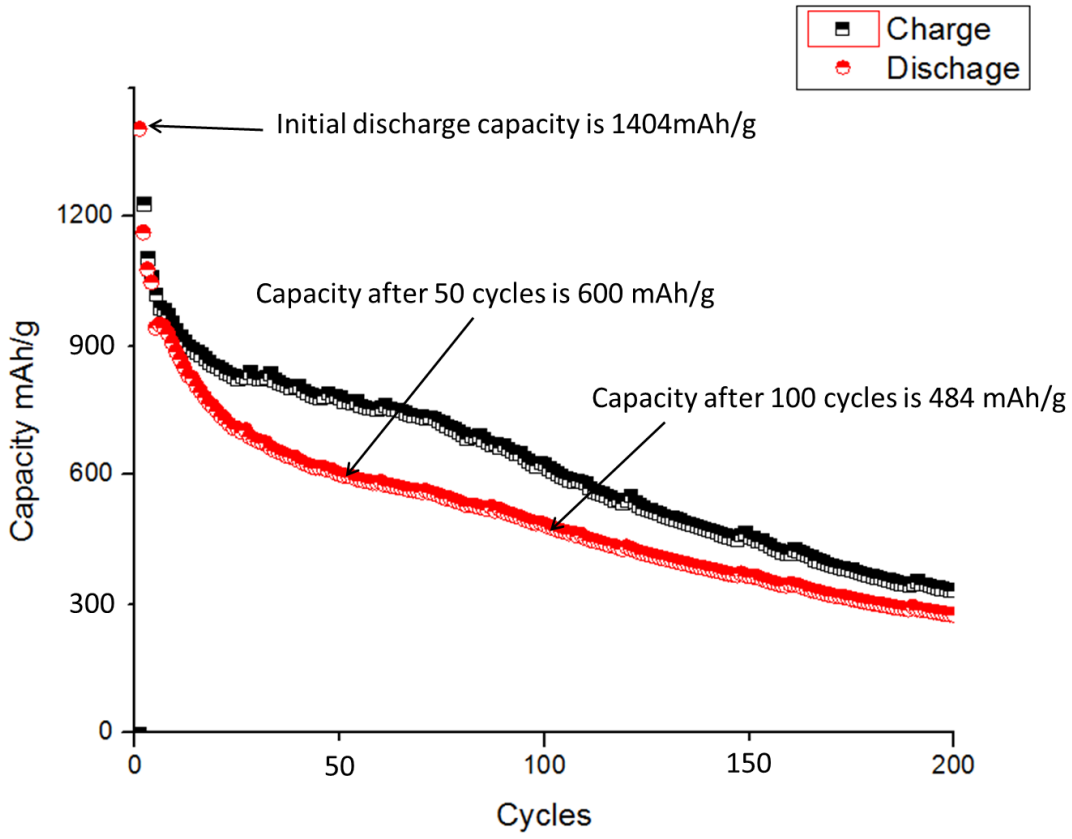

Figure 3.14 Cyclic performance of nanosponge sulfur carbon composite at 0.2C.

The coulombic efficiency is higher than 90% at beginning 10 cycles, and fall down to 76% after 50 cycles. At beginning stage, the closely attached structure delivers a sufficient conductivity contact and extra carbon act as passivation layer to reduce the shuttle effect. At later stage, coulombic efficiency decrease, possibly due to irregular morphology of sulfur shifting. The sulfur cluster to interface between electrode and electrolyte, and naturally carbon passivation layer lost the original morphology.

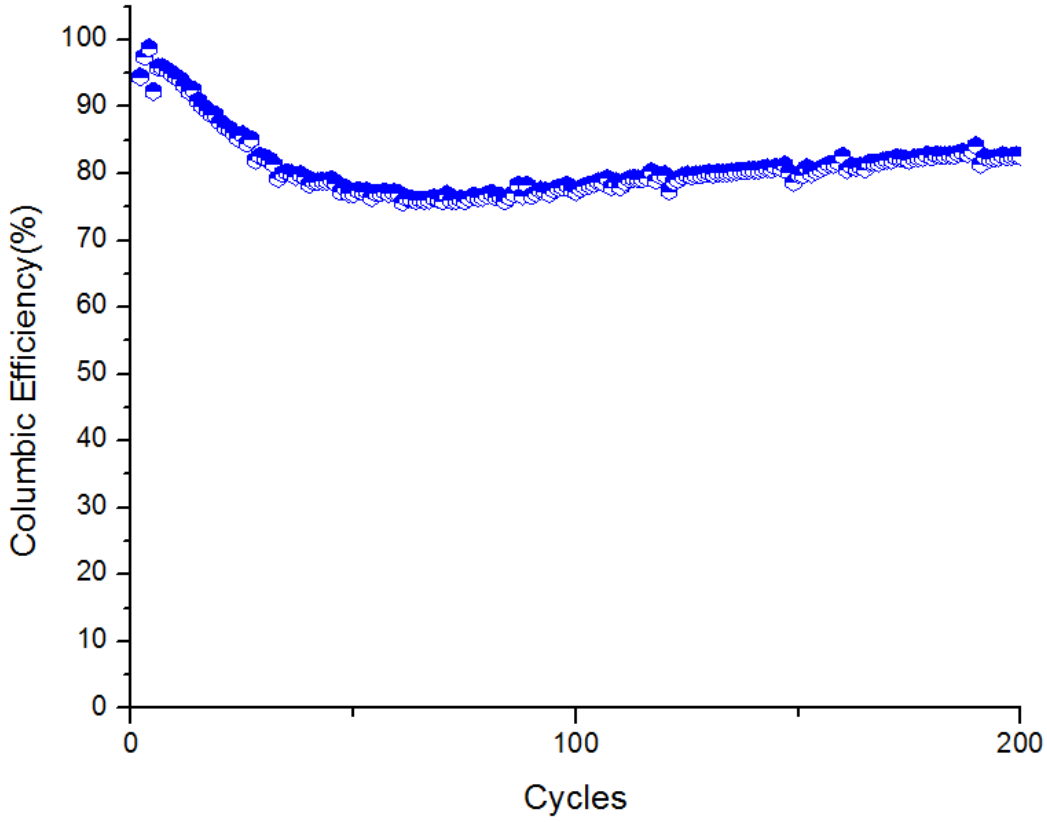

Figure 3.15Coulombic efficiency of nanosponge sulfur carbon composites.

4. Conclusions

Two rational and scalable cathode designs for lithium sulfur batteries were studied in this thesis. For first experiment, sulfur-carbon composites prepared based on reaction between EDA-S precursor and hydrochloric acid. The sulfur particles size can be precisely controlled about 500nm by altering several effect factors. We obtained sulfur carbon composites with sufficient conductive contact and a structure can accommodate volume expansion during discharging/charging process. And we did some necessary characterizations for EDA-S carbon composites cathode materials to determine the morphology and crystal structure via XRD, TEM, and SEM. Meanwhile, we did several electrochemical characterizations for assembled lithium sulfur battery, such as, cyclic voltammetry, cyclic performance and coulombic efficiency. The initial specific capacity of sample is 1032 mAh/g and also capacity can be retained about 200mAh/g after 100 cycles at 0.2C.

Respectively, nanosponge sulfur carbon composite was synthesized by heat treatment process at 155 °C. The XRD and electrochemical characterizations were applied to study nanosponge sulfur carbon materials. The initial discharge capacity starts from 1404 mAh/g at 0.2C and coulombic efficiency is 95%. At 50th cycles, the 600mAh/g remained. The advantages and disadvantages for our synthesized cathode materials also were discussed based on how to overcome shuttle effect, enhancing the electrical conductivity and to accommodate the volume expansion.

References

1. Whittingham, M. S., Electrical Energy Storage and Intercalation Chemistry. *Science* 1976, *192*, 4244.

2. Nitta, N.; Yushin, G., High-Capacity Anode Materials for Lithium-Ion Batteries: Choice of Elements and Structures for Active Particles. *Particle & Particle Systems Characterization* 2014, *31* (3), 317-336.

3. Wu, H.; Cui, Y., Designing nanostructured Si anodes for high energy lithium ion batteries. *Nano Today* 2012, *7* (5), 414-429.

4. (a) Szczech, J. R.; Jin, S., Nanostructured silicon for high capacity lithium battery anodes. *Energy Environ. Sci.* 2011, *4* (1), 56-72; (b) Yoo, J. K.; Kim, J.; Lee, H.; Choi, J.; Choi, M. J.; Sim, D. M.; Jung, Y. S.; Kang, K., Porous silicon nanowires for lithium rechargeable batteries. *Nanotechnology* 2013, *24* (42), 424008; (c) Liu, N.; Wu, H.; McDowell, M. T.; Yao, Y.; Wang, C.; Cui, Y., A yolk-shell design for stabilized and scalable li-ion battery alloy anodes. *Nano Lett* 2012, *12* (6), 3315-21.

5. Kim, H.; Seo, M.; Park, M. H.; Cho, J., A critical size of silicon nano-anodes for lithium rechargeable batteries. *Angewandte Chemie* 2010, *49* (12), 2146-9.

6. Choi, S.; Jung, D. S.; Choi, J. W., Scalable fracture-free SiOC glass coating for robust silicon nanoparticle anodes in lithium secondary batteries. *Nano letters* 2014, *14* (12), 7120-5.

7. Courtney, I. A., J. Electrochem. Soc. 1997, *144* (6), 2045.

8. Xu, L.; Kim, C.; Shukla, A. K.; Dong, A.; Mattox, T. M.; Milliron, D. J.; Cabana, J., Monodisperse Sn nanocrystals as a platform for the study of mechanical damage during electrochemical reactions with Li. *Nano Lett* 2013, *13* (4), 1800-5.

9. Dahn, I. A. C. a. J. R., Electrochemical and In Situ X-Ray Diffraction Studies of the Reaction of Uthium with Tin Oxide Composites. *J. Electrochem. Soc.* 1997, *2045*, 52.

10. (a) Goriparti, S.; Miele, E.; De Angelis, F.; Di Fabrizio, E.; Proietti Zaccaria, R.; Capiglia, C., Review on recent progress of nanostructured anode materials for Li-ion batteries. *Journal of Power Sources* 2014, *257*, 421-443; (b) Yoshio Idota, T. K., Akihiro Matsufuji, Yukio Maekawa, Tsutomu Miyasak, Tin-Based Amorphous Oxide: A High-Capacity Lithium-lon-Storage Materia. *Science* 1997, *276*, 1395.

11. Li, H.; Wang, Z.; Chen, L.; Huang, X., Research on Advanced Materials for Li-ion Batteries. *Advanced Materials* 2009, *21* (45), 4593-4607.

12. Jiang, J.; Li, Y.; Liu, J.; Huang, X.; Yuan, C.; Lou, X. W., Recent advances in metal oxide-based electrode architecture design for electrochemical energy storage. *Adv Mater* 2012, *24* (38), 5166-80.

13. Zhou, X.; Wan, L. J.; Guo, Y. G., Binding SnO2 nanocrystals in nitrogen-doped graphene sheets as anode materials for lithium-ion batteries. *Adv Mater* 2013, *25* (15), 2152-7.

14. Wang, Z.; Zhou, L.; David Lou, X. W., Metal Oxide Hollow Nanostructures for Lithium-ion Batteries. *Advanced Materials* 2012, *24* (14), 1903-1911.

15. Yang, Z.; Du, G.; Guo, Z.; Yu, X.; Li, S.; Chen, Z.; Zhang, P.; Liu, H., Plum-branch-like carbon nanofibers decorated with SnO2 nanocrystals. *Nanoscale* 2010, *2* (6), 1011-7.

16. Jalem, R.; Mochiduki, Y.; Nobuhara, K.; Nakayama, M.; Nogami, M., Global minimum structure search in Li(x)CoO2 composition using a hybrid evolutionary algorithm. *Physical chemistry chemical physics : PCCP* 2012, *14* (37), 13095-100.

17. Kraytsberg, A.; Ein-Eli, Y., Higher, Stronger, Better… A Review of 5 Volt Cathode Materials for Advanced Lithium-Ion Batteries. *Advanced Energy Materials* 2012, *2* (8), 922-939.

18. Hassoun, J.; Bonaccorso, F.; Agostini, M.; Angelucci, M.; Betti, M. G.; Cingolani, R.; Gemmi, M.; Mariani, C.; Panero, S.; Pellegrini, V.; Scrosati, B., An advanced lithium-ion battery based on a graphene anode and a lithium iron phosphate cathode. *Nano letters* 2014, *14* (8), 4901-6.

19. Niu, J.; Kushima, A.; Qian, X.; Qi, L.; Xiang, K.; Chiang, Y. M.; Li, J., In situ observation of random solid solution zone in LiFePO(4) electrode. *Nano letters* 2014, *14* (7), 4005-10.

20. Kushima, A.; Koido, T.; Fujiwara, Y.; Kuriyama, N.; Kusumi, N.; Li, J., Charging/Discharging Nanomorphology Asymmetry and Rate-Dependent Capacity Degradation in Li-Oxygen Battery. *Nano letters* 2015, *15* (12), 8260-5.

21. Zhong, L.; Mitchell, R. R.; Liu, Y.; Gallant, B. M.; Thompson, C. V.; Huang, J. Y.; Mao, S. X.; Shao-Horn, Y., In situ transmission electron microscopy observations of electrochemical oxidation of Li2O2. *Nano letters* 2013, *13* (5), 2209-14.

22. Ma, Z.; Yuan, X.; Li, L.; Ma, Z.-F.; Wilkinson, D. P.; Zhang, L.; Zhang, J., A review of cathode materials and structures for rechargeable lithium–air batteries. *Energy Environ. Sci.* 2015, *8* (8), 2144-2198.

23. Manthiram, A.; Fu, Y.; Chung, S. H.; Zu, C.; Su, Y. S., Rechargeable lithium-sulfur batteries. *Chemical reviews* 2014, *114* (23), 11751-87.

24. Ji, X.; Lee, K. T.; Nazar, L. F., A highly ordered nanostructured carbon-sulphur cathode for lithium-sulphur batteries. *Nature materials* 2009, *8* (6), 500-6.

25. Aurbach, D.; Pollak, E.; Elazari, R.; Salitra, G.; Kelley, C. S.; Affinito, J., On the Surface Chemical Aspects of Very High Energy Density, Rechargeable Li–Sulfur Batteries. *Journal of*

The Electrochemical Society 2009, *156* (8), A694.

26. Su, Y. S.; Fu, Y.; Cochell, T.; Manthiram, A., A strategic approach to recharging lithium-sulphur batteries for long cycle life. *Nature communications* 2013, *4*, 2985.

27. Niu, J.; Kushima, A.; Li, M.; Wang, Z.; Li, W.; Wang, C.; Li, J., Scalable synthesis of a sulfur nanosponge cathode for a lithium–sulfur battery with improved cyclability. *J. Mater. Chem. A* 2014, *2* (46), 19788-19796.

28. Chen, H.; Wang, C.; Dong, W.; Lu, W.; Du, Z.; Chen, L., Monodispersed sulfur nanoparticles for lithium-sulfur batteries with theoretical performance. *Nano letters* 2015, *15* (1), 798-802.

29. Wei Seh, Z.; Li, W.; Cha, J. J.; Zheng, G.; Yang, Y.; McDowell, M. T.; Hsu, P. C.; Cui, Y., Sulphur-TiO2 yolk-shell nanoarchitecture with internal void space for long-cycle lithium-sulphur batteries. *Nature communications* 2013, *4*, 1331.